

# Plug-In Voltage Dip Compensation Using Mainstream Shunt Grid-Connected Converters

**Citation for published version (APA):**

Zhang, Y., Xu, X., Duarte, J. L., & Fei, W. (2021). Plug-In Voltage Dip Compensation Using Mainstream Shunt Grid-Connected Converters. In *2020 IEEE 9th International Power Electronics and Motion Control Conference (IPEMC2020-ECCE Asia)* (pp. 663-668). Article 9368187 Institute of Electrical and Electronics Engineers. <https://doi.org/10.1109/IPEMC-ECCEAsia48364.2020.9368187>

**DOI:**

[10.1109/IPEMC-ECCEAsia48364.2020.9368187](https://doi.org/10.1109/IPEMC-ECCEAsia48364.2020.9368187)

**Document status and date:**

Published: 09/03/2021

**Document Version:**

Accepted manuscript including changes made at the peer-review stage

**Please check the document version of this publication:**

- A submitted manuscript is the version of the article upon submission and before peer-review. There can be important differences between the submitted version and the official published version of record. People interested in the research are advised to contact the author for the final version of the publication, or visit the DOI to the publisher's website.
- The final author version and the galley proof are versions of the publication after peer review.
- The final published version features the final layout of the paper including the volume, issue and page numbers.

[Link to publication](#)

**General rights**

Copyright and moral rights for the publications made accessible in the public portal are retained by the authors and/or other copyright owners and it is a condition of accessing publications that users recognise and abide by the legal requirements associated with these rights.

- Users may download and print one copy of any publication from the public portal for the purpose of private study or research.
- You may not further distribute the material or use it for any profit-making activity or commercial gain
- You may freely distribute the URL identifying the publication in the public portal.

If the publication is distributed under the terms of Article 25fa of the Dutch Copyright Act, indicated by the "Taverne" license above, please follow below link for the End User Agreement:

[www.tue.nl/taverne](http://www.tue.nl/taverne)

**Take down policy**

If you believe that this document breaches copyright please contact us at:

[openaccess@tue.nl](mailto:openaccess@tue.nl)

providing details and we will investigate your claim.

# Plug-In Voltage Dip Compensation Using Mainstream Shunt Grid-Connected Converters

Ya Zhang  
Prodrive Technologies B.V.  
Eindhoven, the Netherlands  
0000-0002-0674-4321

Xinwei Xu, Jorge Duarte  
Department of Electrical Engineering  
Eindhoven University of Technology  
Eindhoven, the Netherlands  
0000-0002-6063-5927, 0000-0003-3208-3747

Fei Wang  
School of Mechatronic Engineering and  
Automation  
Shanghai University, Shanghai, China  
f.wang@shu.edu.cn

**Abstract**—Voltage dips may cause adverse effects to connected devices. Series and shunt grid-connected converters have been developed to compensate voltage amplitude variations. However, existing compensation approaches either rely on information of load current or external reactive power reference. In this paper, a voltage dip compensation strategy, which requires local measurements only, is proposed. This approach enables mainstream shunt grid-connected converters, which have no external current sensors, to compensate voltage dips (and swells) in distribution grids. A converter prototype is built and tested to verify the proposed compensation strategy.

**Keywords**—grid-connected converter, dynamic voltage restorer, voltage dip compensation

## I. INTRODUCTION

Similar to voltage unbalance and harmonics in distribution grid, voltage dips may cause device malfunction to end-users [1, 2]. Voltage dip compensators, also known as dynamic voltage restorers, has been widely adopted to mitigate voltage dips in distribution grids. A common configuration of dynamic voltage restorers is by connecting a converter in series with the grid, as shown in Fig. 1 (a) [3, 4]. Operating as a voltage source, the converter generates voltage difference between the grid voltage and the nominal voltage required by the load. An alternative configuration is by connecting a converter in parallel with the grid [5-8], as shown in Fig. 1 (b). In this case, the converter injects suitable amount of current to the grid based on the level of the voltage dip. This current introduces voltage increment across the line impedance, which is relatively high in a weak grid.

Voltage dip compensation (VDC) based on series connected converter (see Fig. 1 (a)) is a direct approach. However, all load current that flows through one of the winding of the transformer also flows into the converter. This means that the series converter needs to provide at least the same power rating as that of the load, making it a customized solution. Although proven possible [9], series-connected converter generally experiences difficulties to deliver active power to grid.

Alternatively, voltage quality compensation using shunt converters has been receiving growing attentions [5-8]. However, experimental investigation is absent in [7]. In [8],

The work described in this paper is within the PROGRESSUS project, which has received funding from the ECSEL Joint Undertaking (JU) under the Grant Agreement No. 876868. The JU receives support from the European Union's Horizon 2020 research and innovation program, as well as from Germany, the Netherlands, Spain, Italy, Slovakia.

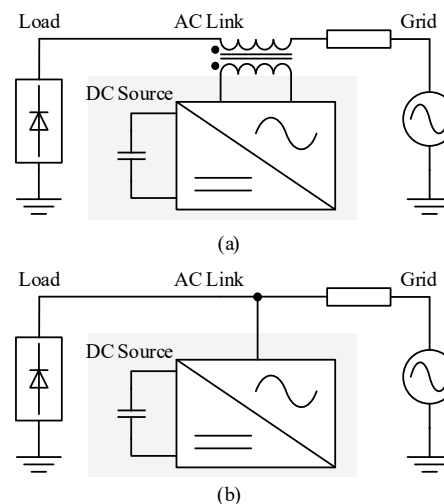


Fig. 1: Configuration of grid-connected converter for voltage dip compensation: (a) series connection, (b) parallel connection.

load information is required to generate a set point for the controller, which makes external sensors necessary. The work in [6] demonstrates that reactive power injection helps to increase voltage fundamental positive-sequence component (PSC) at the point of common coupling (PCC). Unfortunately, no details are given on how to calculate the reactive power reference. A localized strategy is presented in [8] to correct the PCC voltage fundamental PSC. However, consideration to the current rating of the converter is not provided.

This paper presents a localized VDC control strategy for mainstream three-phase grid-connected converters, either of three-phase four-wire configuration or of three-phase three-wire configuration, as shown in Fig. 2. This VDC strategy consists of reactive current generation, fundamental PSC voltage RMS value detection, and reactive current amplitude reference calculation. It decouples VDC control and active power regulation. The diagram of the proposed control strategy is shown in Fig. 3. A synchronous reference frame phase-locked-loop (SRF-PLL) [10-12] is adopted to derive the phase of the fundamental PSC of the PCC voltage. The plug-in voltage dip compensation in the grey box is an add-on to conventional active power regulation of grid-connected converters. In addition, beside voltage dip compensation, the strategy also



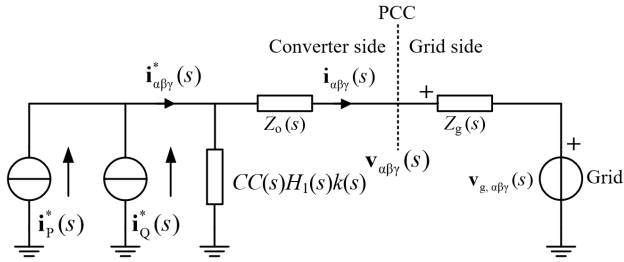


Fig. 4: Circuit diagram showing reactive current injection from the GCC.

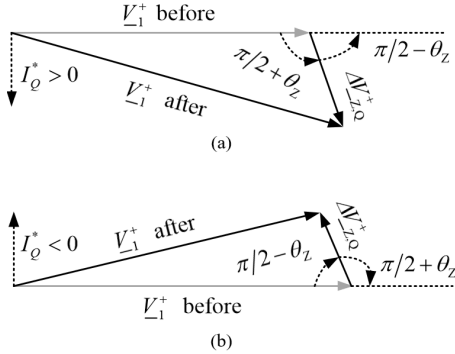


Fig. 5: Phasor diagram of PCC voltage modification: (a) voltage dip compensation (b) voltage swell compensation.

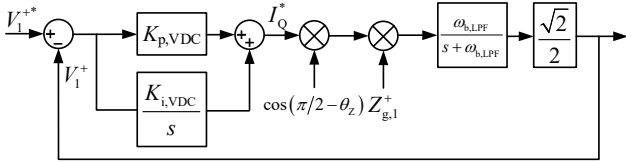


Fig. 6: Linear model of the voltage dip compensation loop.

Table 1: Parameters of current loop controller

Parameter	Symbol	Value
Proportional gain	$K_{p,CC}$	3
Integrator gain	$K_{i,CC}$	120
Resonance filter gain for the $n^{\text{th}}$ harmonic component	$K_{res,n}$	$2000/n^2$
Harmonic orders under compensation	$h$	3,5,7
Damping factor	$\zeta$	0.001

According to Fig. 3, the current reference of  $\gamma$  component is zero, which removes zero-sequence current injection. Since this paper focuses on regulation of PSCs for PCC voltage dip compensation, only  $\alpha\beta$  components are discussed in the following.

Equation (5) is represented by an equivalent circuit diagram (see Fig. 4) for the ease of demonstration. The circuit contains a voltage source  $V_{g,\alpha\beta}(s)$ , two current source  $i_p^*$ ,  $i_Q^*$ , converter output impedance  $Z_o$ , and grid line impedance  $Z_g$ . The current loop creates a virtual impedance,  $CC(s)H_1(s)k(s)$ , which is in series with the converter output impedance.

In this paper, the current controller is designed to have high gains at fundamental and low-order grid-harmonic frequencies. The transfer function of  $CC(s)$  is expressed as

$$CC(s) = K_{p,CC} + K_{i,CC} \frac{1}{s} + \sum_{n \in h} K_{res,n} \frac{2s}{s^2 + 2\zeta n\omega_1 s + (n\omega_1)^2} \quad (6)$$

where  $K_{p,CC}$ ,  $K_{i,CC}$ ,  $K_{res,n}$ ,  $h$ , and  $\zeta$  are proportional gain, integrator gain, resonance filter gain for the  $n^{\text{th}}$  harmonic component, harmonic orders under compensation, and damping factor respectively. The parameters of the current controller are summarized in Table 1.

Due to high loop gain at fundamental and some harmonic frequencies, the converter output current is insensitive to grid voltage  $v_{g,\alpha\beta}$ , and is mainly determined by the fundamental PSC current reference  $i_p^*$  and  $i_Q^*$ .

### III. REACTIVE POWER AND PCC VOLTAGE

According to [6], reactive power injection increases the fundamental PSC magnitude of PCC voltage. However, calculation of reactive power reference is not provided. In this section, a strategy that flexibly increases and decreases the PCC voltage is presented.

The phasor diagram in Fig. 5 demonstrates the process of PCC voltage modification, which explains the mechanism of voltage dip and swell compensation by reactive power injection. The phasor of the fundamental PSC of the PCC voltage (before compensation,  $I_Q^* = 0$ ) is denoted as  $V_{-1}^+$ . The induced voltage drop on the grid impedance  $Z_g$  due to reactive current injection is designated as  $\Delta V_{Z,Q}^+$ . The grid impedance phase angle for the fundamental PSC is referred as  $\theta_z$ .

Since an injected reactive current lags the PCC voltage by  $\pi/2$ , when  $I_Q^* > 0$ , the voltage drop over the grid impedance lags the PCC voltage by  $\pi/2 - \theta_z$ , as shown in Fig. 5 (a). When  $I_Q^* < 0$ , it leads the PCC voltage by  $\pi/2 + \theta_z$ , as shown in Fig. 5 (b). Due to the fact that the grid impedance is mostly inductive for low-order harmonic frequencies [14], the PCC voltage is increased under positive reactive power injection and decreased under negative reactive power injection.

### IV. MODELLING AND DESIGN OF VOLTAGE DIP COMPENSATION LOOP

With reference to Fig. 4, the PCC voltage fundamental PSC is modelled based on the grid voltage and the reactive current injection by

$$\underbrace{V_1^+ e^{j\theta_{PCC}}}_{V_1^+} = \underbrace{V_{g,1}^+ e^{j\theta_g} + Z_{g,1}^+ e^{j\theta_z} I_p^* e^{j\theta_{PCC}}}_{V_{-1}^+ \text{ (before)}} + \underbrace{Z_{g,1}^+ e^{j\theta_z} I_Q^* e^{j(\theta_{PCC} - \pi/2)}}_{\Delta V_{Z,Q}^+} \quad (7)$$

where  $V_1^+$  is the magnitude of the PCC voltage fundamental PSC, and  $\theta_{PCC}$  is its phase. Above,  $I_p^*$ ,  $I_Q^*$ , and  $V_{g,1}^+$  are all amplitudes. After some arrangements, (7) becomes

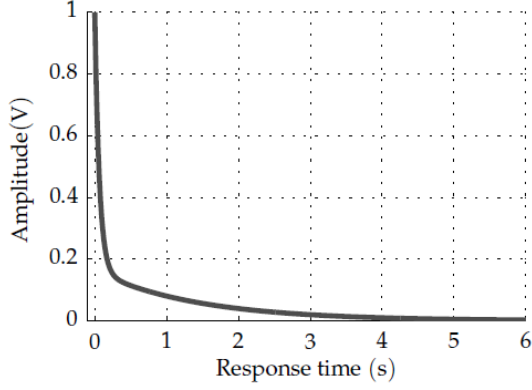


Fig. 7: Close loop step response (from input to error) of the voltage dip compensation.

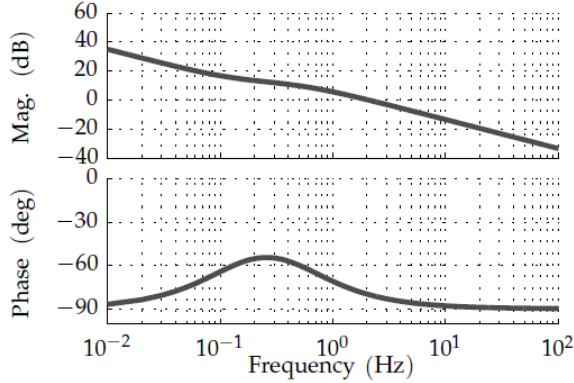


Fig. 8: Bode plot of the voltage dip compensation loop gain  $H_{o,VDC}(s)$ .

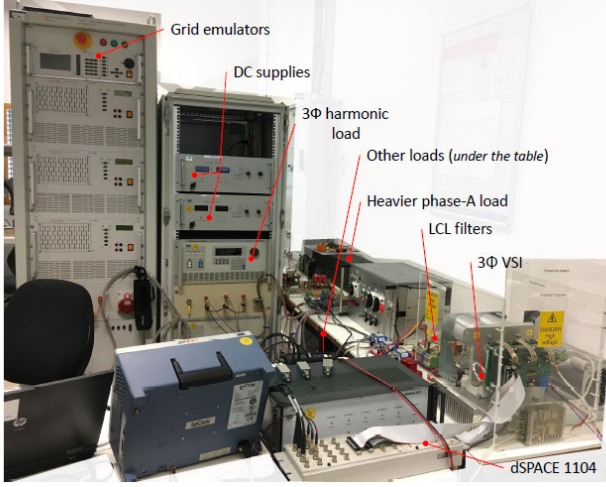


Fig. 9: Photograph of the A three-phase grid-connected converter

$$V_1^+ = V_{g,1}^+ e^{j(\theta_g - \theta_{PCC})} + Z_{g,1}^+ e^{j\theta_z} I_p^* + Z_{g,1}^+ I_Q^* e^{j(\theta_z - \pi/2)} \quad (8)$$

Since the induced voltage drop in the grid line impedance is much smaller than the grid voltage, the dynamics introduced from PLL is ignored. Therefore, the voltage dip compensation loop is linearized as shown in the control loop diagram in Fig. 6. According to [14], the grid line impedance for low-order harmonic frequencies lie between resistive and inductive,

namely  $0 \leq \theta_z \leq \pi/2$ . For stability analysis of the voltage dip compensation loop, the highest loop gain is considered by assuming  $\cos(\pi/2 - \theta_z) = 1$ . The open loop gain of the VDC loop is expressed as

$$H_{o,VDC}(s) = \frac{\sqrt{2}}{2} Z_{g,1}^+ \left( K_{p,VDC} + K_{i,VDC} \frac{1}{s} \right) \frac{\omega_{b,LPF}}{s + \omega_{b,LPF}} \quad (9)$$

with  $Z_{g,1}^+ = \omega_1 L_g$ , where  $\omega_1$  is the grid angular frequency and  $L_g$  is the grid inductance.

Table 2: Parameters of voltage dip compensation loop

Parameter	Symbol	Value
Fundamental angular frequency	$\omega_1$	$100\pi$ rad/s
Bandwidth of VDC loop	$\omega_{b,VDC}$	$\omega_1/25$
Bandwidth of LPF	$\omega_{b,LPF}$	$\omega_1/1000$
Proportional gain	$K_{p,VDC}$	3
Integrator gain	$K_{i,VDC}$	2.5

By selecting the bandwidth of the VDC loop as  $\omega_{b,VDC}$ , the proportional gain is

$$K_{p,VDC} = \left| \frac{\sqrt{2}}{Z_{g,1}^+ \left( 1 + \frac{K_{i,VDC}}{j\omega_{b,VDC}} \right)} \frac{j\omega_{b,VDC} + \omega_{b,LPF}}{\omega_{b,LPF}} \right|, \quad (10)$$

where  $\omega_{b,LPF}$  is the bandwidth of the low pass filter (LPF). The integrator gain is chosen in a way that the phase margin of the VDC loop is  $100^\circ$ . Table 2 summarizes the VDC loop control parameters, from which a closed loop step response (from input to error) and the open loop Bode plot are derived as shown in Fig. 7 and Fig. 8 .

## V. EXPERIMENTAL VERIFICATION

In order to verify the proposed voltage dip compensation strategy, several experimental tests are performed. Fig. 9 shows the grid-connected converter system under test. With reference to Fig. 2, the specifications of the converter system is summarized in Table 3.

Table 3: Specifications of the three-phase grid-connected converter

Specification	Symbol	Value
DC power supply	$V_{dc}$	200 V
Switching frequency	$f_{sw}$	11 kHz
Grid frequency	$f_g$	50 Hz
Grid voltage phase-to-neutral	$V_g$	110 V <sub>rms</sub>
Converter-side inductor	$L_1$	3.6 mH (ESR 0.2Ω)
Filter capacitor	$f_g$	10 μF (ESR 0.2Ω)
Grid-side inductor	$L_2$	2.0 mH (ESR 0.2Ω)
Grid inductor	$L_g$	6.0 mH (ESR 0.4Ω)

### A. PCC voltage dip/swell compensation

The nominal grid phase-to-neutral voltage is set to be

$$V_1^{*+} = 110 V_{rms}. \quad (11)$$

This value is used as the reference for the PCC voltage

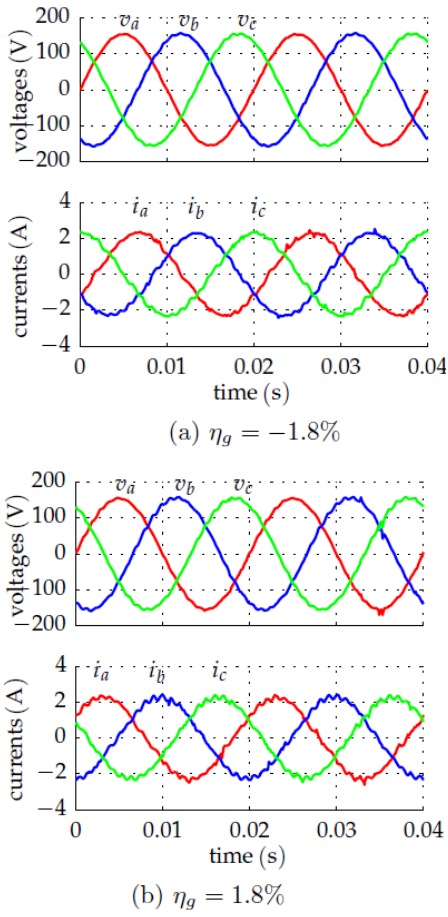


Fig. 10: PCC voltage and converter output current waveforms under voltage dip compensation test: the grid voltage is (a) below the nominal (b) above the nominal.

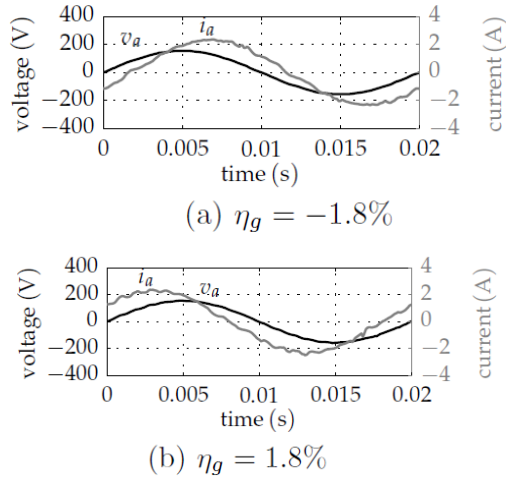


Fig. 11: PCC voltage and converter output current waveform of phase A under voltage dip compensation test: the grid voltage is (a) below the nominal (b) above the nominal.

fundamental PSC, as shown in Fig. 3. For the ease of description, two indexes,

$$\begin{cases} \eta_{\text{PCC}} = \frac{V_1^+}{V_1^{+*}} - 1 \\ \eta_g = \frac{V_{g,1}^+}{V_1^{+*}} - 1 \end{cases}, \quad (12)$$

are introduced to quantify the voltage variation level of the PCC voltage and the grid voltage. Above,  $\eta_{\text{PCC}}$  denotes the dip level of the PCC voltage, while  $\eta_g$  represents the variation level of the grid voltage.

The waveforms of the converter output current and the PCC voltage when the grid voltage amplitude deviates from its nominal value is shown in Fig. 10. The active current reference is set to  $I_p^* = 2 \text{ A}$ . In Fig. 10 (a), since the grid voltage magnitude is smaller than the set value, a positive reactive current ( $I_Q^* > 0$  in Fig. 5 (a)) is generated. This makes the converter output current lag the PCC voltage, as the waveforms of phase A shown in Fig. 11 (a).

In Fig. 10 (b), a negative reactive current ( $I_Q^* < 0$  in Fig. 5 (b)) is generated to compensate the extra grid voltage magnitude. This reactive current creates a voltage drop across the line impedance, which is almost in anti-phase of the grid voltage. In this case, the converter output current leads the PCC voltage (see Fig. 11 (b)). The PCC voltage variation of  $\eta_g = -1.8\%$  and  $\eta_g = 1.8\%$  can be found in Fig. 12, which shows that in both cases the PCC voltage dip is removed completely.

Fig. 12 shows the experimental results of the PCC voltage dip compensation when the grid voltage is deviated from its nominal value. As shown, the VDC loop removes the PCC voltage dip/swell completely when the grid voltage variation level  $\eta_g$  is within  $[-2.5\%, 2.5\%]$ . When the grid voltage deviation exceeds  $\pm 2.5\%$ , the converter still contributes to the PCC voltage support. However, the voltage dip/swell is compensated partially. Due to the limited capacity of the converter system under test, a saturator which limits the reactive current amplitude reference to  $[-2 \text{ A}, 2 \text{ A}]$  is added as shown in Fig. 3.

### B. Dynamic performance

In this section, transient steps are added to the grid voltage and the active current reference to test the dynamic performance of the proposed voltage dip compensation algorithm on a three-phase grid-connected converter.

The experimental waveforms of the converter under grid voltage transient are shown in Fig. 13. The grid voltage steps from  $100 \text{ V}_{\text{rms}}$  to  $108 \text{ V}_{\text{rms}}$  at 0.5 s, which corresponds to the variation of  $\eta_g$  from 0% to -1.8%. At the beginning of the transient, the PCC voltage variation index  $\eta_{\text{PCC}}$  is negative. Afterwards, the PCC voltage dip is eliminated because of the increased injection of reactive current.

Fig. 14 shows the experimental waveforms of the converter under active current reference transient. The current reference  $I_p^*$  steps from 2 A to 3 A at 0.5 s. This temporarily increases the PCC voltage, resulting a positive  $\eta_{\text{PCC}}$ . With the help of the

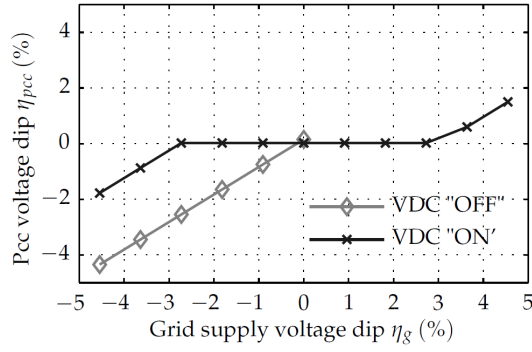


Fig. 12: PCC voltage compensation under a wide range of grid voltage variation.

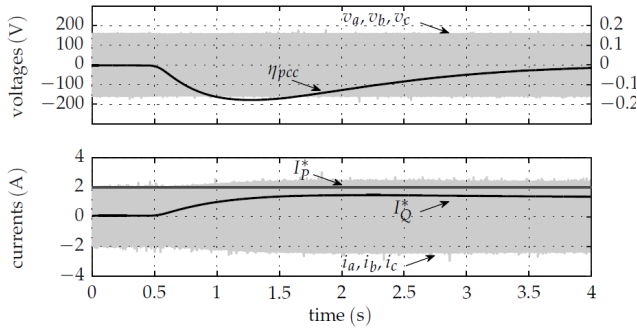


Fig. 13: Dynamic performance of the PCC voltage dip compensation under grid voltage transient (from 110 V to 108 V, i.e.,  $\eta_g$  steps from 0 to -1.8%) at 0.5 s.

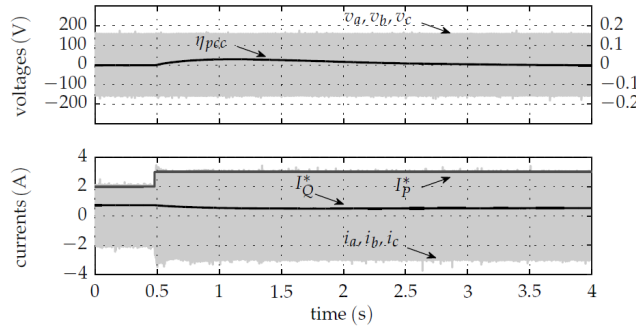


Fig. 14: Dynamic performance of the PCC voltage dip compensation under active current reference transient (from 2 A to 3 A) at 0.5 s.

VDC loop, the reactive current injection is reduced to counteract the increased PCC voltage.

Both in Fig. 13 and Fig. 14, the PCC voltage variation are settled within around 3 s, which is consistent to the analytical result in Fig. 7. Therefore, the proposed VDC algorithm functions well under transient conditions and has a good dynamic performance.

## VI. CONCLUSION

This paper proposes a plug-in voltage dip compensation algorithm for shunt grid-connected converters. The VDC algorithm does not require information on load current. In addition, the VDC loop is decoupled from that of the active

power regulation. The reactive current reference is calculated based on the measured PCC voltage, the desired PCC voltage, and the current rating of the converter system.

Experimental tests are carried out to verify the proposed algorithm. When the grid voltage deviates from its nominal value with a certain range, the converter completely corrects the voltage variation. When the grid voltage exceeds that range, the converter output reactive current is saturated by default. Nevertheless, it still contributes to the reduction of PCC voltage dip or swell.

## VII. REFERENCES

- [1] G. Ye, Y. Xiang, V. Cuk, and J. F. G. Cobben, "Voltage dip state estimation in distribution networks by applying Bayesian inference," in *IECON 2015 - 41st Annual Conference of the IEEE Industrial Electronics Society*, 2015, pp. 000915-000920.
- [2] D. V. Hertem, M. Didden, J. Driesen, and R. Belmans, "The optimal selection of mitigation methods against voltage dips and interruptions: a customer-based approach," in *2004 11th International Conference on Harmonics and Quality of Power (IEEE Cat. No.04EX951)*, 2004, pp. 631-636.
- [3] F. M. Mahdianpoor, R. A. Hooshmand, and M. Ataei, "A New Approach to Multifunctional Dynamic Voltage Restorer Implementation for Emergency Control in Distribution Systems," *IEEE Transactions on Power Delivery*, vol. 26, pp. 882-890, 2011.
- [4] C. N. Ho, H. S. H. Chung, and K. T. K. Au, "Design and Implementation of a Fast Dynamic Control Scheme for Capacitor-Supported Dynamic Voltage Restorers," *IEEE Transactions on Power Electronics*, vol. 23, pp. 237-251, 2008.
- [5] C. Xu, K. Dai, X. Chen, and Y. Kang, "Unbalanced PCC voltage regulation with positive- and negative-sequence compensation tactics for MMC-DSTATCOM," *IET Power Electronics*, vol. 9, pp. 2846-2858, 2016.
- [6] Z. Dai, H. Lin, H. Yin, and Y. Qiu, "A novel method for voltage support control under unbalanced grid faults and grid harmonic voltage disturbances," *IET power Electronics*, vol. 8, pp. 1377-1385, 2015.
- [7] M. Bongiorno and J. Svensson, "Voltage Dip Mitigation Using Shunt-Connected Voltage Source Converter," *IEEE Transactions on Power Electronics*, vol. 22, pp. 1867-1874, 2007.
- [8] A. Ashourpour, M. Dargahi, and S. A. N. Niaki, "Residential voltage dip and swell mitigation using Plug-in Hybrid Electric Vehicle in smart grid," in *2013 Australasian Universities Power Engineering Conference (AUPEC)*, 2013, pp. 1-5.
- [9] N. Saadat, S. S. Choi, and D. M. Vilathgamuwa, "A Series-Connected Photovoltaic Distributed Generator Capable of Enhancing Power Quality," *IEEE Transactions on Energy Conversion*, vol. 28, pp. 1026-1035, 2013.
- [10] K. Zhou, Y. Yang, F. Blaabjerg, and D. Wang, "Optimal Selective Harmonic Control for Power Harmonics Mitigation," *IEEE Transactions on Industrial Electronics*, vol. 62, pp. 1220-1230, 2015.
- [11] Q.-N. Trinh and H.-H. Lee, "An enhanced grid current compensator for grid-connected distributed generation under nonlinear loads and grid voltage distortions," *IEEE Transactions on Industrial Electronics*, vol. 61, pp. 6528-6537, 2014.
- [12] O. J. K. Oghorada and L. Zhang, "Unbalanced and Reactive Load Compensation Using MMCC-Based SATCOMs With Third-Harmonic Injection," *IEEE Transactions on Industrial Electronics*, vol. 66, pp. 2891-2902, 2019.
- [13] Y. Zhang, M. Roes, M. Hendrix, and J. Duarte, "Symmetric-component decoupled control of grid-connected inverters for voltage unbalance correction and harmonic compensation," *International Journal of Electrical Power & Energy Systems*, vol. 115, p. 105490, 2020.
- [14] J. Sun, "Impedance-based stability criterion for grid-connected inverters," *IEEE Transactions on Power Electronics*, vol. 26, pp. 3075-3078, 2011.